ARTICLE NO. 79-7020R

Calculation of the Flow Properties of a Confined Kerosene-Spray Flame

Y. El Banhawy* and J. H. Whitelaw†
Imperial College of Science and Technology, London, U.K.

A calculation procedure for the prediction of local properties of spray flames is described and evaluated by comparison with experimental data. The mathematical formulation comprises the application of Eulerian conservation equations to the gas phase and Lagrangian equations of droplet motion and thermal balance to a small finite number of droplet size ranges representing the size-distribution within the spray. The latter is coupled with a droplet-tracking technique which allows the determination of the droplet location and properties within the flowfield. The spray combustion model assumes that the evaporating droplets act as distributed point injectors of fuel vapor within the flame, and that the combustion rate of fuel vapor is controlled by the turbulent transport from the vapor and oxidant streams. Experimental and predicted results are shown to be in qualitative agreement, and the comparison emphasizes the importance of the spray initial conditions, including the shape of the size distribution and the droplets' initial velocity. Compared to the turbulence and combustion models, the number of size ranges was tested in the range between 5 and 20 and found not to be important for the spray considered.

Nomenclature

c_p = specific heat under constant pressure, J/kg K
D_p = droplet diameter, m
f = mixture fraction
g = square of the fluctuation of concentration
H_{fu} = fuel heat of reaction, J/kg_{fuel}
K_f = thermal conductivity of gases, J/m K kg
L = fuel latent heat of vaporization, J/kg
P = pressure, N/m^2
T = temperature, K
U = axial velocity component, m/s
V = radial velocity component, m/s
W = tangential velocity component, m/s
μ = viscosity, kg/m·s
ρ = density

Subscripts

f = gas-phase
p = droplet
v = vapor
eff = effective (including the effects of turbulence)

Introduction

THE prediction of the hydrodynamic and thermal characteristics of spray flames requires consideration of the two phases in the flowfield which are coupled through exchange processes of mass, heat, and momentum. The main mathematical burden is associated with the modeling of the discontinuous liquid-phase and the coupling between the two phases. Moreover, the modeling of the combustion process requires consideration of the spray characteristics, which act as additional combustion-rate controlling parameters.

The problem of predicting the local flow properties in situations where a spray of droplets is injected in a turbulent gas field has been investigated by Crowe,[1] Crowe et al.,[2] and Sharma.[3] Eulerian conservation equations were applied to the gas phase with the assumption of insignificant influence of local flow discontinuities induced by the presence of droplets in the gas phase. Lagrangian equations of droplet motion and thermal balance equations were applied to a finite number of droplet size ranges representing the size distribution within the spray. The interaction between the two phases was accounted for by considering the droplets as sources of mass, heat, and momentum to the gas field.

A different approach was developed by Williams,[4] who modeled the spray through a conservation equation for a statistical distribution function, defined as the number of droplets per unit droplet diameter, and velocity and spatial volume. The influence of the spray on the gas field was considered through source terms, representing different exchange processes, included in the conservation equations of the gas field. The main difficulty associated with this approach lies in the solution of the final set of equations which have an integrodifferential character. Application of the method was described in Refs. 5 and 6.

Harlow et al.[7] and Gosman et al.[8] used the continuum formulation of the conservation equations, for both phases, to predict local gas and particle properties in a range of flow geometries. Fluid properties, which vary rapidly on a scale comparable with the particle spacing, were replaced by smoothed variables obtained by averaging over regions which were large compared with the particle spacing, but small compared with the complete system. The resulting equations described the motion of the fluid and particles as though they were interpenetrating continua. There is much argument in the literature concerning the validity of the continuum assumption under different flow conditions (see, e.g., Ref. 9) and the modeling of the turbulent stress tensor for the liquid or solid phase. Assessment of the procedure by applying it to simple two-phase flow problems is, therefore, required prior to its application to the more complex spray flows.

The present paper describes a calculation method for the prediction of reacting sprays with a mathematical approach based on that of Crowe[1] for nonreacting sprays. The ability of the present procedure to predict the local properties of spray flames is demonstrated by comparison with the experimental data of Ref. 10, obtained for a range of confined swirling spray flames. The comparison indicates general

Presented as Paper 79-7020 at the 4th International Symposium on Airbreathing Engines, Walt Disney World, Fla., April 1-6, 1979; submitted Aug. 22, 1979; revision received March 31, 1980.

Index categories: Combustion and Combustor Designs; Computational Methods; Multiphase Flows.

*Research Assistant, Mechanical Engineering Dept., Fluids Section.

†Professor of Convective Heat Transfer, Mechanical Engineering Dept., Fluids Section.

agreement with measurements, but deficiencies remain and are attributed mainly to uncertainties in the calculated spray evaporation and spreading rates and to the two-equation turbulence model associated with the prediction of strongly recirculating flow.

Mathematical Analysis of the Gas Field

The conservation equations for the turbulent gas field are derived for time-averaged dependent variables, and the turbulent shear stresses are calculated with a two-equation (for the kinetic energy k and its dissipation rate ϵ) turbulence model.[11] For two-dimensional turbulent, axisymmetric, combusting, and steady gas flow with recirculation, the governing equations can all be written in the same general form,[12] i.e.,

$$\frac{\partial}{\partial x}(\rho_f U_f \phi) + \frac{1}{r}\frac{\partial}{\partial r}(r\rho_f V_f \phi) = \frac{\partial}{\partial x}\left\{\Gamma\frac{\partial \phi}{\partial x}\right\} + \frac{1}{r}\frac{\partial}{\partial r}\left\{r\Gamma\frac{\partial \phi}{\partial r}\right\} + S + S_d \quad (1)$$

where ϕ is any one of the dependent variables, and the exchange coefficient Γ and source term S stand for expressions assembled in Table 1; S_d is the term representing the interaction between the fuel droplets and gases and is obtained from the solution of droplet-field equations as will be described later. Equation (1) is solved with the eight dependent variables indicated in Table 1 and the pressure correction equation referred to in the numerical solution procedure. It is assumed that the fuel droplets do not influence the turbulent structure other than through the release of thermal energy, i.e., the droplet concentration is small.

Combustion Model

The spray combustion model used in this paper is based on the assumption that liquid droplets act as distributed sources of fuel vapor within the spray. The implication is that chemical reaction in spray flames can be treated in a way similar to that used for turbulent gaseous diffusion flames. Experimental evidence for this assumption can be found in Refs. 13-15. Several combustion models for gaseous diffusion flames are reported in the literature (see, e.g., Refs. 16 and 17). The combustion model for the present calculations assumes that fuel and oxygen burn instantaneously in a one-step reaction and can coincide at the same point, but at different times, according to a double-delta function probability distribution.[16] This model has been appraised in connection with gaseous flames (see, e.g., Ref. 17) and can probably be improved by the incorporation of an alternative probability-distribution assumption; it has, however, been shown to yield reasonable results for a range of gas flames.

Spray Model

The present model assumes that the fuel is injected into the combustion chamber as a fully atomized spray which consists of spherical droplets. The droplet-size distribution within the spray is represented by a finite number of size ranges, as shown in Fig. 1, with the correlation equation from Ref. 18, i.e.,

$$\frac{dn}{n} = A\left(\frac{D}{D_{32}}\right)^{\alpha} e^{-B(D/D_{32})^{\beta}} \frac{dD}{D_{32}}$$

where dn and n are the number of droplets in the size range from D to $D+dD$ and the total number of droplets, respectively; D_{32} is the Sauter mean diameter; and α, β, A, and B are experimentally determined constants.

For each size range, droplet trajectories, velocities, size, and temperature history within the combustion chamber are obtained by solving the momentum and thermal balance equations for the droplet representing this size range.

The solution of the governing equations for the gas field incorporates a finite-difference procedure where a staggered-grid is used to divide the flowfield into computation cells for the application of the conservation principles (see Ref. 12 and Fig. 2). The knowledge of the droplet properties (size, velocity, number, etc.) at the cell boundaries allows the calculation of the loss or gain of the droplet mass, heat, and momentum within each cell, which appears as source or sink terms in the corresponding finite-difference equations for the gas phase. These source terms represent the coupling link between the droplet and gas fields.

The calculation of the droplet-source terms require knowledge of the rate of the number of droplets entering and leaving each calculation cell; it is assumed that the number of droplets associated with each size range is constant along its trajectory, and this implies that turbulent diffusion of droplets and the effects of droplet collision and breakup are neglected.

Mathematical Analysis of the Droplet Field

The coupling between the droplet and gas fields, through the droplet-source terms, necessitates the determination of the droplet location, size, temperature, and velocity within the combustion chamber. This is done by tracking different droplets throughout their movement inside the calculation domain; consequently, a Lagrangian framework is used to describe the droplet behavior.

Momentum Balance Equations

For each droplet representing a size range, the momentum balance equations (see, e.g., Ref. 9) are written as

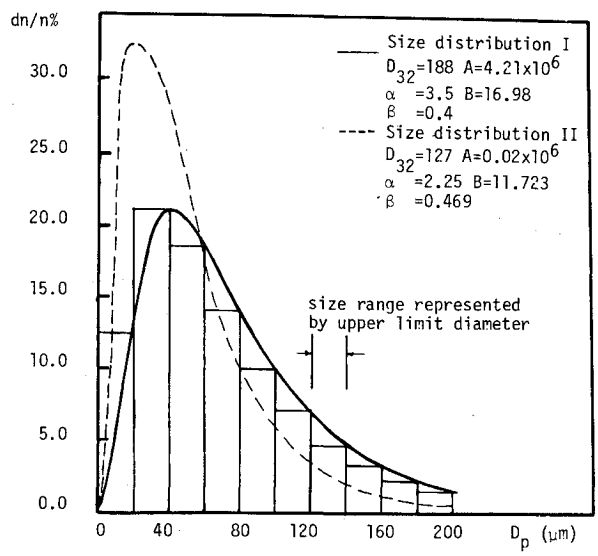

Fig. 1 Droplet size distributions.

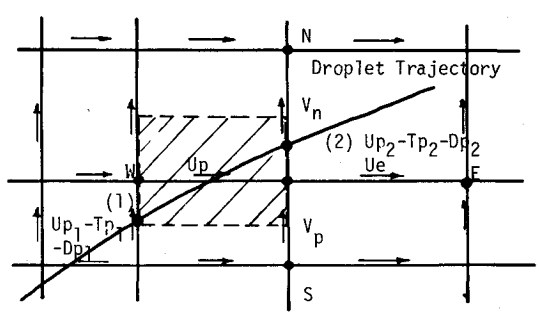

Fig. 2 Computation cells and droplet trajectory.

Axial direction

$$\frac{dU_p}{dt} = -\frac{1}{\rho_p}\left(\frac{\partial p}{\partial x}\right)_f + \frac{6\cdot\mu}{\pi\rho_p\cdot D_p^2}(U_f - U_p)f(Re_\ell) \quad (2)$$

Radial direction

$$\frac{dV_p}{dt} - \frac{W_p^2}{y_p} = -\frac{1}{\rho_p}\left(\frac{\partial p}{\partial y}\right)_f + \frac{6\cdot\mu}{\pi\rho_p D_p^2}(V_f - V_p)f(Re_\ell) \quad (3)$$

Tangential direction

$$\frac{dW_p}{dt} + \frac{V_p\cdot W_p}{y_p} = \frac{6\cdot\mu}{\pi\rho_p D_p^2}(W_f - W_p)f(Re_\ell) \quad (4)$$

The drag function is given by $f(Re_\ell) = \pi/8\cdot C_d\cdot Re_\ell$, where Re_ℓ is a Reynolds number of the droplets defined as

$$Re_\ell \equiv \frac{\rho_f\cdot D_p\cdot|(\bar{U}_f - \bar{U}_p)|}{\mu}$$

Several correlations for the drag coefficient C_d can be found in the literature (see, e.g., Refs. 19 and 20). A correlation which has been used by several investigators and found to be reasonably accurate is used in the present work,[19] i.e.,

$$C_D = 27\cdot Re_\ell^{-0.84} \qquad 0 < Re_\ell < 80$$
$$= 0.271\cdot Re_\ell^{0.217} \qquad 80 < Re_\ell < 10^4$$
$$= 2.0 \qquad Re_\ell < 10^4$$

The effects of evaporation and droplet distortion on C_D are included implicitly in the preceding correlation.

Droplet-Size-Change Expression

The mass transfer rate from the liquid to the gas phase associated with evaporation[21] is given by

$$\dot{m}_p = 2\pi D_p\frac{K_f}{cp_f}\ell n(1+B) \quad (5)$$

where the transfer number B is $B = cp_v(T_f - T_{sat})/L$ and has been derived for evaporation from single droplets but without chemical reaction.

$\dot{m}_p$ can also be expressed as

$$\dot{m}_p = \frac{\pi}{2}\rho_p D_p^2\frac{dD_p}{dt} \quad (6)$$

and, from Eqs. (5) and (6), dD_p/dt can be expressed as

$$\frac{dD_p}{dt} = \frac{-4\cdot K_f}{\rho_p\cdot cp_f}\frac{1}{D_p}\ell n(1+B) = \frac{-32}{D_p}K_e$$

where K_e is the evaporation rate constant for stagnant conditions. For moving droplets, K_e is corrected by the following expression (see, e.g., Ref. 19):

$$K_{eff} = 0.5xK_e x(2.0 + 0.56Re_\ell^{0.5})$$

Then,

$$\frac{dD_p}{dt} = \frac{-2K_f}{\rho_p cp_f}(2 + 0.56Re_\ell^{0.5})\ell n(1+B)\frac{1}{D_p} \quad (7)$$

Thermal Balance Equation

The droplet temperature during the preheating period (prior to the start of evaporation) is determined by solving the thermal balance equation for a droplet moving in a gas stream. By assuming that the prevailing mode of heat transfer is forced convection, no evaporation takes place during the preheating period, and that the temperature is uniform across the droplet radius, the resulting thermal balance equation is

$$\frac{dT_p}{dt} = \frac{6}{D_p\rho_p c_p}h(T_f - T_p) \quad (8)$$

where h is the heat transfer coefficient,[19] i.e.,

$$h = N_u K_f/D_p = (K_f/D_p)(2.0 + 0.56R_{e_\ell}^{0.5})$$

and N_u is the Nusselt number. Equation (8) is solved only during the preheating period, and the droplet temperature during subsequent movement will be that corresponding to saturation.

Equations (2-4), (7), and (8) represent a closed set of equations which, with appropriate initial conditions and knowledge of gas properties, provide the variation of the droplet velocity, size, and temperature in the time domain. The corresponding droplet properties in the space domain are obtained by the droplet-tracking technique described in a following section.

Numerical Solution Procedure

Gas Field

The gas phase elliptic partial differential equations, together with the boundary conditions, are solved by a finite-difference procedure through the TEACH-code computer program.[12] The finite-difference form of Eq. (1) is derived by integration over a cell surrounding the variable under consideration and is solved numerically with the dependent variables $U_f, V_f, W_f, h, f, g, k$, and ϵ of Table 1.

The velocity field calculated from the momentum equation is linked to corrections to the pressure-field to satisfy the continuity equation. These corrections are obtained from a pressure correction equation derived from both the continuity and momentum equations in the manner described by Caretto et al.[22] This equation is modified to account for mass coupling between the droplet and gas field, as described in Ref. 1.

The droplet-gas coupling is incorporated in the numerical procedure as follows. An isothermal, droplet-free solution of the gas field is first obtained, then droplet trajectories, size, and temperature history are calculated through the droplet-field equations with known gas properties. The droplet source terms are then calculated for each cell in the calculation domain and fed to the finite-difference form of Eq. (1) to obtain adjusted values for the dependent variables. These are used again in the solution of the droplet-equations. This process of solving the gas field equations followed by the droplet equations is repeated until all the equations are satisfied.

Droplet Field

The simultaneous differential Eqs. (2-4), (7), and (8) for the droplet behavior are solved numerically using a Runge-Kutta-4 method.

Droplet Tracking

The numerical procedure used to solve the droplet-equations provides the axial, radial, and tangential velocity components at the start and end of each time-step. These velocity components are used through a tracking method to determine the position of the droplets relative to the gas-field where the following relations are used (see Fig. 2):

$$X_{end} = X_{start} + 0.5(U_{start} + U_{end})\Delta t$$

$$Y_{end} = Y_{start} + 0.5(V_{start} + V_{end})\Delta t$$

Table 1 Expressions appearing in Eq. (1)

Variable ϕ	Γ	S
U_f	μ_{eff}	$\frac{\partial}{\partial x}\left(\mu_{\text{eff}}\frac{\partial U_f}{\partial x}\right)+\frac{1}{r}\frac{\partial}{\partial r}\left(\mu_{\text{eff}} r\frac{\partial V_f}{\partial x}\right)-\frac{\partial p}{\partial x}$
V_f	μ_{eff}	$\frac{\partial}{\partial x}\left(\mu_{\text{eff}}\frac{\partial U_f}{\partial r}\right)+\frac{1}{r}\frac{\partial}{\partial r}\left(\mu_{\text{eff}} r\frac{\partial V_f}{\partial r}\right)-\frac{2\mu V_f}{r^2}+\frac{W_f^2}{r}-\frac{\partial P}{\partial r}$
W_f	μ_{eff}	$-\left(\frac{\mu_{\text{eff}}}{r^2}+\frac{V_f}{r}+\frac{1}{r}\frac{\partial \mu_{\text{eff}}}{\partial r}\right)W_f$
k	$\frac{\mu_{\text{eff}}}{\sigma_k}$	$G_{k_1}-\epsilon^{a}$
ϵ	$\frac{\mu_{\text{eff}}}{\sigma_\epsilon}$	$\frac{\epsilon}{k}(C_1 G_{k_1}-C_2\epsilon)$
f	$\frac{\mu_{\text{eff}}}{\sigma_f}$	0
$\bar{h}$	$\frac{\mu_{\text{eff}}}{\sigma_h}$	0
g	$\frac{\mu_{\text{eff}}}{\sigma_g}$	$C_{g_1}\cdot G_{g_2}\frac{\epsilon}{k}\cdot g^{b}$

$$^{a}G_{k_1}=\mu_{\text{eff}}\left|2\left(\left(\frac{\partial U_f}{\partial x}\right)^2+\left(\frac{\partial V_f}{\partial r}\right)^2+\left(\frac{V_f}{r}\right)^2+\left(\frac{\partial W_f}{\partial x}\right)^2+\left(\frac{r\partial}{\partial r}\left(\frac{W_f}{r}\right)\right)^2+\left(\frac{\partial U_f}{\partial r}+\frac{\partial V_f}{\partial x}\right)^2\right|$$

$$^{b}G_{g_1}=\mu_{\text{eff}}\left|\left(\frac{\partial f}{\partial x}\right)^2+\left(\frac{\partial f}{\partial r}\right)^2\right|$$

σ = effective turbulent Prandtl number for the variables ϕ = 0.9. $C_1 = 1.44$ and $C_2 = 1.92$ are constants of the turbulence model. $C_{G_1} = 2.8$ and $C_{G_2} = 2.0$ are constants of the concentration fluctuations, Eq. (g).

Droplet properties at the end of the time-step are stored at X_{end} and Y_{end}. The swirling fuel spray is assumed to be axisymmetric. Hence, although the droplets are moving in a spiral-like motion, their position is identified only by the two coordinates X and Y. The time step used in the calculation has been chosen to give the time-step independent solution for the droplet equations. The treatment of droplets impinging on the combustion chamber walls is important in modeling spray flames. On impingement, droplets may form a liquid film, shatter, or reflect with reduced momentum, and the rules which govern the choice of these alternatives are not well formulated. Thus, a simple assumption has been made here, namely, if a droplet arrives at a surface, the calculation proceeds by assigning a negative value for the radial velocity component and reducing the three velocity components by a factor accounting for the loss of momentum upon impingement (a value of 0.85 has been used in the present calculations).

Interaction Source Terms

Droplet tracking allows the size, velocity, and position of the droplet to be determined in the calculation domain. Droplet source terms are obtained by calculating the loss or gain of the droplet mass and momentum within each cell. Summing up the respective source terms for droplets representing different size ranges gives the total droplet source terms.

The mass exchange rate between the droplet and gases in a cell is given by the following expression[1]:

$$S_{dM}=\sum_{L=1}^{N}(\dot{m}_{di}-\dot{m}_{do})_L$$

where $\dot{m}_{di}$ and $\dot{m}_{do}$ are the mass fluxes of the droplet at entry and exit to the cell, respectively; N is the total number of size ranges representing the sray; and $\dot{m}_{dL}=\pi/6\cdot\rho_p\cdot D_{pL}^3\dot{n}_L\cdot\dot{n}_L$ is the number of droplets issuing from the spray nozzle per unit time and with diameters corresponding to the size range L.

For the axial momentum, the momentum exchange rates are given by,

$$S_{dU}=\sum_{L=1}^{N}(M\dot{U}_{do}-M\dot{U}_{di})_L$$

where $M\dot{U}_{do}$ and $M\dot{U}_{di}$ are the axial momentum fluxes of the droplet at exit and entry to the cell, respectively, and $\dot{M}U_{dL}=\pi/6\rho_p D_{pL}^3\cdot U_{pL}\cdot\dot{n}_L$. Similarly,

$$S_{dV}=\sum_{L=1}^{N}(M\dot{V}_{do}-M\dot{V}_{di})_L$$

and

$$S_{dW}=\sum_{L=1}^{N}(M\dot{W}_{do}-M\dot{W}_{di})_L$$

The total enthalpy exchange rate is given by

$$S_{dH}=\sum_{L=1}^{N}(\dot{m}_{di}-\dot{m}_{do})(H_{\text{fu}}-L)$$

Calculated Results

The present calculation procedure has been tested by applying it to predict the local flow properties in a confined,

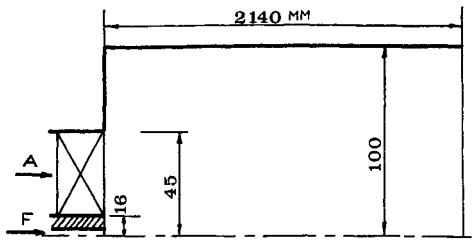

Fig. 3 Geometry of the combustion chamber.

Table 2 Spray inlet conditions for the test cases

Case No.	Number of size ranges	Size distribution[a]	Injection velocity[b]
1	10	I	A
2	5	II	A
3	10	I	B
4	5	I	A
5	20	I	A

[a] Size-distribution of droplets:

$$\mathrm{I} \equiv \frac{dn}{n} = 4.21\times10^{6}\left(\frac{D_p}{188}\right)^{3.5}\exp\left(-16.98\left(\frac{D_p}{188}\right)^{0.4}\right)\frac{dD}{188}$$

$$\mathrm{II} \equiv \frac{dn}{n} = 0.0203\times10^{6}\left(\frac{D_p}{127}\right)^{2.252}\exp\left(-11.723\left(\frac{D_p}{127}\right)^{0.469}\right)\frac{dD}{127}$$

[b] Injection velocity of droplets: $A \equiv U_p = 11.0$, $W_p = 6.1$, V_p varies from 0.5-2.5, the small value corresponds to smallest droplet-diameter. $B \equiv U_p = 10.0$, $W_p = 2.0$, V_p varies from 0.5-2.5, the smallest value corresponds to smallest droplet-diameter.

swirling spray flame. The geometry of the combustion chamber is shown in Fig. 3. Experimental data for temperature, axial, and tangential velocity components were obtained from Ref. 10 and correspond to the following inlet conditions: air mass flow rate = 355 kg/h, air/fuel ratio = 20.17, swirl number = 0.721, swirler vane angle = 45 deg, inlet air axial velocity = 15 m/s, air temperature at entry = 310 K.

A fuel nozzle of the swirl-atomization type was used in the experimental tests. The spray droplet-size distribution corresponding to the preceding operating conditions is shown in Fig. 1, and the inlet conditions used in the present calculations are given in Table 2.

The calculations were performed with a grid of 20×20 nodes which allowed the solution of the complete set of equations, including the solution of the droplet equations for 10 size ranges, in approximately 14 min of CDC 6600 time. In the test case where 5 and 20 size ranges were considered, the computing time was 12 and 18 min, respectively. They were performed for five cases, corresponding to the spray inlet conditions summarized in Table 2, and allowed examination of the influence of the spray inlet conditions, including size-distribution, injection velocities, and the number of size ranges, on the predicted results. The presentation of the results first allows a comparison of the experimental and predicted results, case 1, and then separate consideration of the influence of each of the preceding variables.

The experimental and predicted results for the axial velocity and temperature profiles at different axial distances from the burner are shown in Fig. 4 and correspond to case 1. The results show that the predicted temperatures are well below the measured values, close to the burner and at small radii of the combustion chamber $r/r_0 < 0.5$, and comparatively high close to the combustion chamber wall. Related discrepancies exist in the corresponding axial velocity profiles. The axial velocity profiles also indicate underprediction of the size and strength of the central recirculation zone.

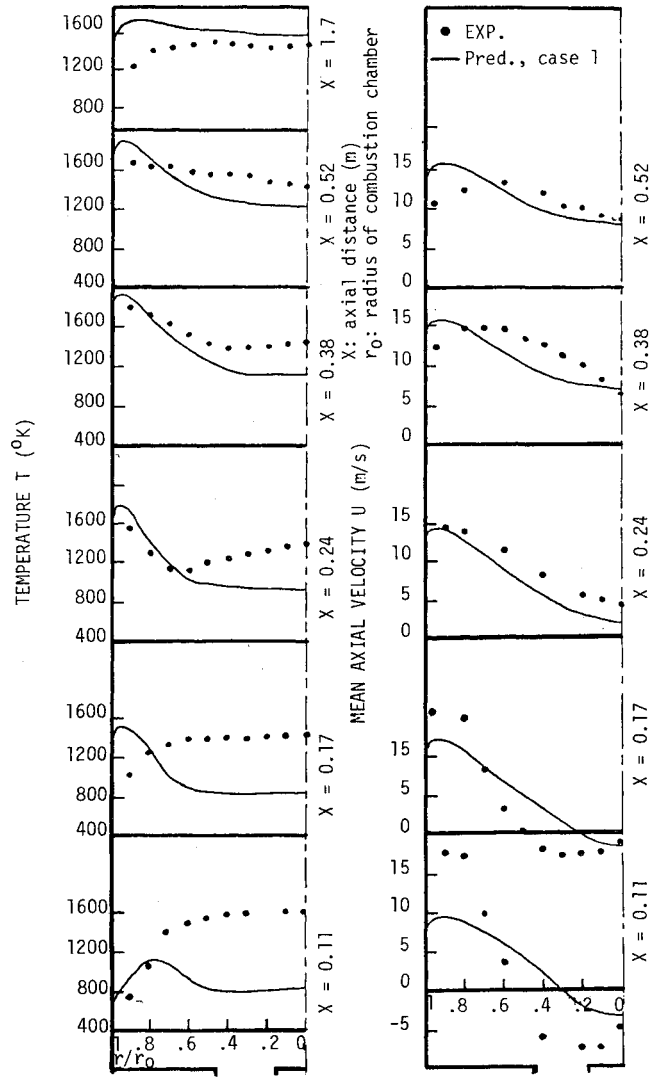

Fig. 4 Radial profiles of temperature and axial velocity for case 1 and experimental results.

The discrepancies in the temperature profiles are influenced by errors in the calculated evaporation and spreading rates of the fuel spray and by the underprediction of the recirculation zone. The distribution of the mass fraction of the evaporated fuel along the combustion chamber is shown in Fig. 5 and indicates that only 80% of the fuel has evaporated by around $x = 0.6$ and that evaporation continues to $x = 1.2$. This slow rate of evaporation may explain the predicted low temperatures in the central part of the upstream sections and the higher temperatures observed downstream. The droplet trajectories of the 10 size ranges showed no significant differences between the trajectories of different size ranges. This suggests an underestimation of the spread of the fuel spray. The trajectories were observed to be concentrated in a small spatial volume which is roughly coincident with the locations of the maxima in the radial temperature distributions of Fig. 4. This is likely to account for the overprediction of temperature at these locations. The uncertainties in the evaporation and spreading rates of the spray are probably related to the assumed spray inlet conditions and to the neglect to the influence of the turbulent gas motion and droplet breakup and collision on the droplet-motion.

Apart from the influence of the underprediction of the recirculation zone on droplet trajectories, it causes a reduction in the amount of hot combustion products recirculated from downstream regions of the flame which, otherwise, would increase the temperature at near-burner

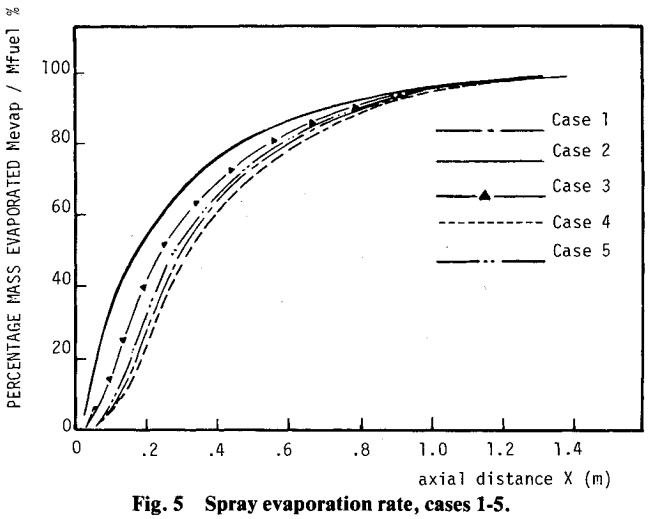

Fig. 5 Spray evaporation rate, cases 1-5.

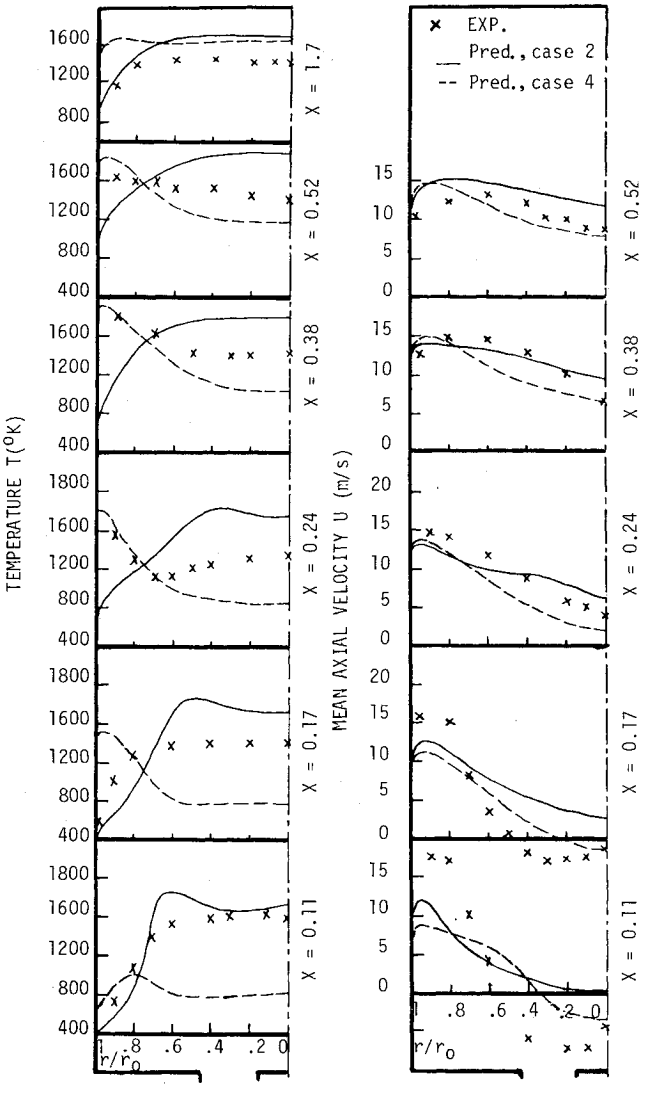

Fig. 6 Radial profiles of temperature and axial velocity for two droplet size distributions.

locations. This has a direct influence on the droplet evaporation and the combustion rate and, therefore, contributes to the low temperatures and evaporation rate at small axial distances. The underprediction of the reverse-velocity zone is associated with uncertainties in the assumed upstream flow boundary conditions and in the two-equation turbulence model employed in the present procedure. The effective-

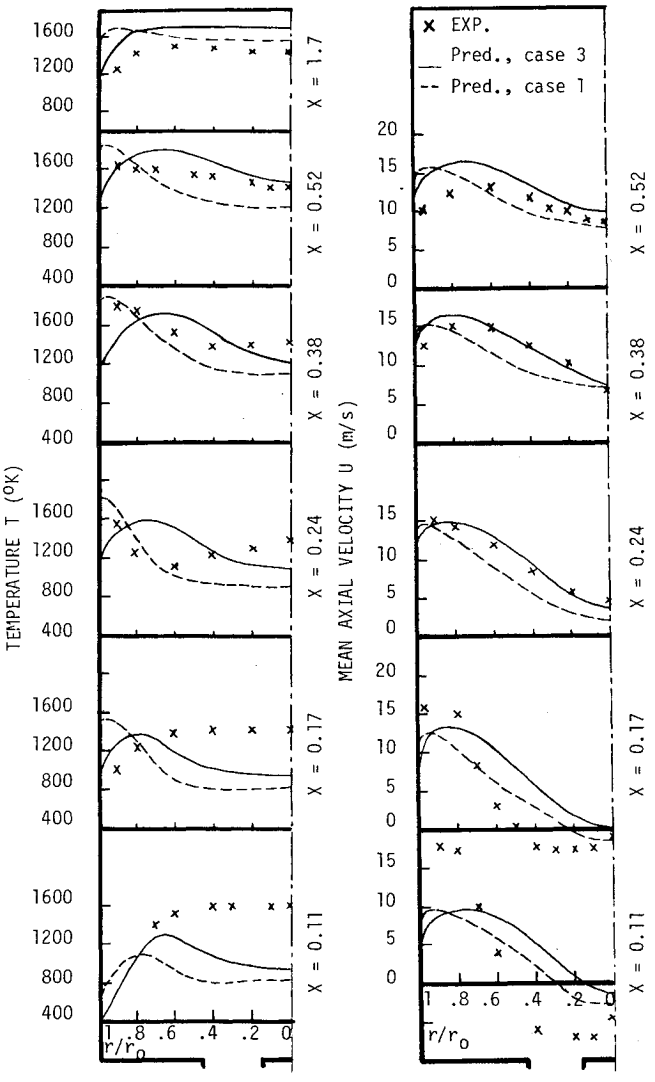

Fig. 7 Radial profiles of temperature and axial velocity for two droplet injection velocities.

viscosity assumption is known[23] to be less precise in highly swirling flows; in addition, the swirl number quoted for the experimental data and used in the present calculations was estimated rather than measured and is subject to some uncertainty.

Radiative heat transfer (see, e.g., Ref. 23) has been omitted from the present calculations mainly for reasons of simplicity. This may cause errors in regions of high temperature and high concentration of absorbing and radiating species and at regions where hot soot particles exist. The neglect of radiation is not, however, expected to be significant compared to the other influences of the spray inlet conditions mentioned previously. For example, in the high-temperature regions, the expected uncertainty in the temperature values (based on previous calculations) will be in the order of 150 K.

The observed discrepancies between the experimental and predicted results should also be related to the uncertainties in the measured temperature and velocity profiles. The temperature was measured by a suction pyrometer with uncertainties of around 10%, which may increase to 15% at regions within the spray boundaries due to droplet impingement on the thermocouple element. The velocity was measured by a 3-hole pitot-tube probe with a maximum error of about 15%.[10]

Influence of Droplet Size Distribution

Calculations were carried out (cases 2 and 4) with the two size distributions of Fig. 1 (see also Table 2). Radial profiles of axial velocity and temperature are presented in Fig. 6 and

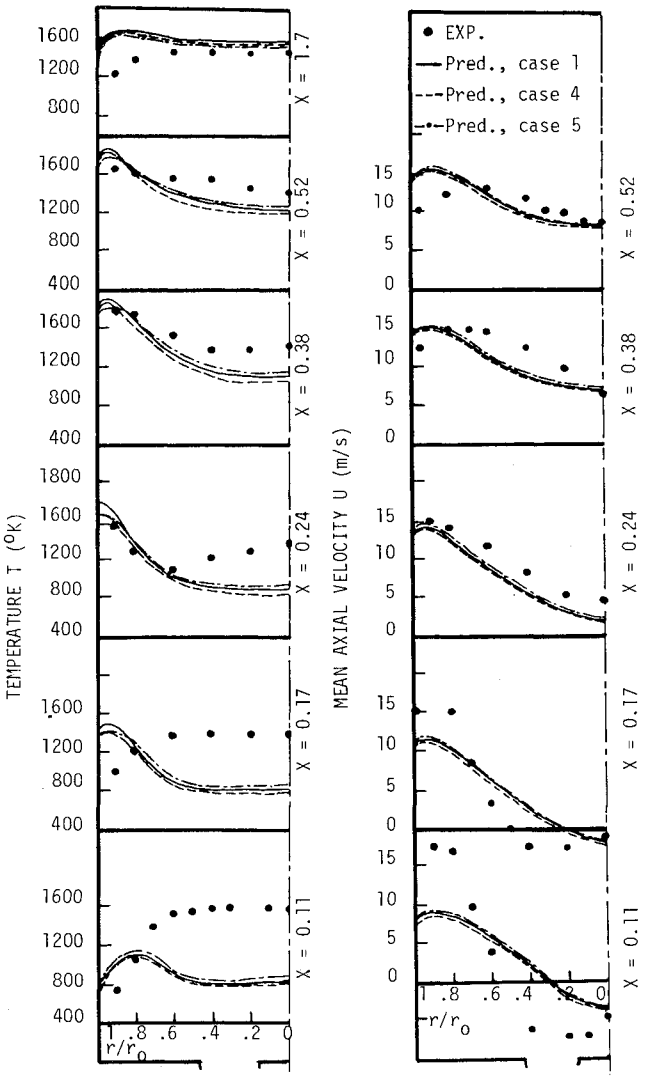

Fig. 8 Radial profiles of temperature and axial velocity for three number of size ranges.

show the influence of shifting the size distribution toward smaller droplet-diameters on the temperature profiles. They indicate the large increase in the temperature values at near-burner locations and around the flame centerline associated with a decrease in temperature at the near-wall region of the downstream sections, e.g., at $x=0.52$. Consequent changes in the axial velocity profiles are indicated in Fig. 6, e.g., the central recirculation zone has completely vanished due partly to the excessive increase in temperature.

The heating period of a droplet and the rate of change of its diameter with time are both inversely proportional to its diameter and, consequently, a reduction in the spray mean-droplet diameter will be associated with earlier droplet evaporation. The increase in the evaporation rate for case 2 is evident from the results of Fig. 5 where, e.g., the mass fraction of the evaporated fuel has increased from 24% (case 4) to 54% (case 2) at $x=0.2$. The increase in the temperature values of case 2 at near-burner and centerline locations is mainly influenced by this rise in the evaporation rate as more fuel is available for combustion in the initial part of the flame. The increase in the evaporation rate in the upstream region is also associated with a reduction in the amount of fuel vapor evolved from fuel droplets during their subsequent movement in the downstream region and close to the chamber wall. This explains the lower temperatures predicted in these regions of the flame for case 2.

It is also likely that the increase in the predicted temperatures within the central part of the flame (case 2) is related to uncertainties in the present combustion model. These stem mainly from the assumptions of a single-step infinitely fast chemical reaction and of the neglect of intermediate reaction species such as carbon monoxide and unburned hydrocarbons. Although concentration measurements were not reported in Ref. 10, the results obtained for similar combustor configurations (see, e.g., Ref. 24) indicate significant concentrations of intermediate species. The neglect of these species, with their comparatively high heats of reaction, results in temperature values which are overestimated. The results of the calculations reported in Ref. 24 suggest that the magnitude of the overestimation in temperature can be as high as 300 K.

Influence of Droplet Injection Velocity

The results of case 1 have been compared with those of case 3 with its lower injection velocity to demonstrate the extent to which changes in the droplet-injection velocity affect the predicted profiles. Radial profiles of axial velocity and temperature are shown in Fig. 7 for the two cases. The temperature profiles of case 3 show an increase in the centerline values associated with a shifting of the location of the radial temperature maxima toward the centerline. This implies an increase in the evaporation rate at small axial distances and a decrease in the spray spreading rate which is confirmed by the results of Fig. 5. The increase in evaporation is due to the increase in the droplets' relative velocity which consequently increase the heat and mass transfer to and from the droplet, respectively.

Influence of the Number of Size Ranges

To demonstrate the influence of the number of size ranges used to represent the spray, calculations were performed for 5 and 20 size ranges (cases 4 and 5) and compared with case 1 (10 size ranges). The predicted results of the axial velocity and temperature profiles are shown in Fig. 8 for the three cases and indicate small differences. An increase in the number of size ranges tends to decrease the differences between the experimental and predicted results, but the magnitude of the change is small. It is likely that, in sprays of the present type (hollow-cone) where the droplets are confined to a small spatial volume, the use of a small finite number of size ranges is sufficient to represent the spray provided that the overall evaporation rate calculated from these size ranges is correctly represented. The distribution of the percentage evaporated mass along the flame is shown in Fig. 5 for the two cases 1 and 5 and indicates insignificant changes in the calculated spray evaporation rate with the number of size ranges.

Concluding Remarks

The reported results of the previous section and the comparison with the experimental data show that general features of the flowfields are correctly predicted by the present procedure. However, quantitative differences exist between the experimental and predicted results particularly at near-burner locations and around the combustion chamber centerline. Consideration of the factors influencing the solution of the droplet-field emphasizes that these discrepancies are mainly related to uncertainties in the calculated spray evaporation and spreading rates. Inspection of the predicted velocity and temperature profiles suggests that the observed deficiencies are related to uncertainties in the initial conditions and in the two-equation turbulence model.

The assumption of representing the spray by a finite number of size ranges has been examined in the present work, and it was shown that increasing the number of size ranges from 5 to 20 causes an average reduction of 5% in the observed errors between the experimental and predicted results. However, the extent to which the results are improved does not justify the increase in computing time. The insignificant

influence of the number of size ranges obtained in the present case is probably due to the fact that in the hollow-cone spray of the present case most droplets follow the same path, and therefore, the use of a small finite number of size ranges will be sufficient to represent the spray provided that the evaporation rate calculated from this finite number is correct.

References

[1] Crowe, C. T., "Gas-Droplet Flowfield in the Vicinity of an Atomizer," *11th JANNAF Combustion Meeting*, Pasadena, Calif., Sept. 1974.

[2] Crowe, C. T., Sharma, M. P., and Stock, D. E., "The Particle-Source-Cell (PSI-CELL) Model for Gas-Droplet Flows," Dept. of Mechanical Engineering, Washington State Univ., Washington, Nov. 1977, pp. 1-30.

[3] Sharma, M. P., "Numerical and Experimental Study of Gas-Particle Flows in Orifices and Venturies," Ph.D. Thesis, Washington State Univ., Washington, Dec. 1977.

[4] Williams, F. A., "Progress in Spray-Combustion Analysis," *8th Symposium (International) on Combustion*, Williams and Wilkins Co., Baltimore, Md., 1962, pp. 50-59.

[5] Gany, A., Mahnheimer-Timnar, T., and Wolfshtein, M., "Two-Phase Flow Effects on Hybrid Combustion," *Acta Astronautica*, Vol. 3, Sept. 1976, pp. 241-263.

[6] Westbrook, C. K., "Three-Dimensional Numerical Modeling of Liquid Fuel Sprays," *16th Symposium (International) on Combustion*, The Combustion Institute, 1977, pp. 1517-1526.

[7] Harlow, F. H. and Amsden, A. A., "Numerical Calculation of Multiphase Fluid Flow," *Journal of Computational Physics*, Vol. 17, Jan. 1975, pp. 19-52.

[8] Gosman, A. D., Li, K. H., and Samaraweera, D.S.A., "A Numerical Calculation Procedure for Two-Phase Recirculating Flows," Mechanical Engineering Dept., Imperial College, London, June 1976.

[9] Hinze, J. O., "Turbulent Fluid and Particle Interaction," Mechanical Engineering Dept., Delft Univ. of Technology, The Netherlands, Rept. WTHD No. 32, Nov. 1971.

[10] Khalil, K. H., El Mahallawy, F. M., and Moneib, H. A., "Effects of Combustion Air Swirl on the Flow Pattern in a Cylindrical Oil-Fired Furnace," *16th Symposium (International) on Combustion*, The Combustion Institute, 1977, pp. 135-143.

[11] Launder, B. E. and Spalding, D. B., *Mathematical Models of Turbulence*, Academic Press, New York, 1972.

[12] Gosman, A. D. and Pun, W. M., Lecture notes for course entitled "Calculation of Recirculating Flows," Mechanical Engineering Dept., Imperial College, London, 1973.

[13] Tuttle, J. H., Shisler, R. A., and Mellor, A. M., "Investigation of Liquid Fueled Turbulent Diffusion Flames," *Combustion Science and Technology*, Vol. 14, Feb. 1976, pp. 229-241.

[14] Onuma, Y., Ogasawara, M., and Inoue, T., "Further Experiments on the Structure of a Spray Combustion Flame," *16th Symposium (International) on Combustion*, The Combustion Institute, 1977, pp. 561-567.

[15] Styles, A. C. and Chigier, N. A., "Combustion of Air Blast Atomized Spray Flames," *16th Symposium (International) on Combustion*, The Combustion Institute, 1977, pp. 619-630.

[16] Spalding, D. B., "Mathematical Models of Turbulent Flames: A Review," *Combustion Science and Technology*, Vol. 13, Feb. 1976, pp. 1-25.

[17] Jones, W. P. and Whitelaw, J. H., "Coupling of Turbulence and Chemical Reaction," Mechanical Engineering Dept., Imperial College, London, 1978, Fluids Section Rept. FS/78/13, (to be published in *Proceedings of U.S. Dept. of Energy Meeting*, Los Angeles, Calif.).

[18] Abu Elleil, M. M., "Theoretical and Experimental Investigation of the Pre-Combustion Period Events of Fuel Droplets in Gas-Turbine Combustion Chambers," Ph.D. Thesis, Cairo University, Cairo, Egypt, June 1974.

[19] Williams, A., "Combustion of Droplets of Liquid Fuels: A Review," *Combustion and Flame*, Vol. 21, 1973, pp. 1-31.

[20] Ingebo, R. D., "Heat Transfer and Drag Coefficients for Ethanol Drops in a Rocket Chamber Burning Ethanol and Liquid Oxygen," *8th Symposium (International) on Combustion*, 1962, pp. 1104-1113.

[21] Spalding, D. B., "The Combustion of Liquid Fuels," *4th Symposium (International) on Combustion*, Williams and Wilkins Co., Baltimore, Md., 1953, pp. 847-864.

[22] Caretto, L. S., Gosman, A. D., Patankar, S. V., and Spalding, D. B., *Proceedings of the 3rd International Conference on Numerical Methods in Fluid Mechanics*, Vol. 2, 1972, p. 60.

[23] Hutchinson, P., Khalil, E. E., and Whitelaw, J. H., "The Measurements and Calculation of Furnace-Flow Properties," *Journal of Energy*, Vol. 1, 1977, p. 212.

[24] El Banhawy, Y. H. and Whitelaw, J. H., "Assessment of an Approach to the Calculation of the Flow Properties of Spray Flames," Paper 12, AGARD CP 275, Feb. 1980.